STM JOURNALS

Journal of
Polymer & Composites

https://journals.stmjournals.com/jopc

ISSN: 2321-2810 (Online)
ISSN: 2321-8525 (Print)
Volume 14, Special Issue 3, 2026
DOI (Journal): 10.37591/JoPC

Research JoPC

Design and Development of Lightweight Polymer Composite Manifold Using CF-ABS and GFRP for Aerodynamic Energy Recovery in Electric Vehicles

Pratik T. Phunde[1], Abhijeet Malge[2], Yogesh Bhalerao[3], Pramod P. Kothmire[4]*

Abstract

Electric vehicles provide a number of advantages over conventional fuel vehicles due to their low to no emissions. High energy efficiency improves the driving performance of Electric vehicles. However, they have to face certain challenges such as the high purchase cost of batteries and lack of battery charging facilities. The major drawback of an Electric vehicle is to store sufficient energy to run the vehicle for a long time. This paper presented a technique to charge the vehicle during its running condition as well as to store the energy generated using renewable sources for the long run. The battery storage capacity is around 1 to 60 kilo Watt hour which is insufficient for covering a one-time traveling distance i.e. around 250 km. The adopted method enhances the traveling range using a secondary power source. This is generated by converting the aerodynamic drag to electrical energy for sustainable transportation. The manifold, a critical flow-directing component, was initially prototyped using Carbon Fiber reinforced ABS (CF-ABS) via additive manufacturing for geometric validation, followed by fabrication in Glass Fiber Reinforced Polymer (GFRP) with epoxy resin for the final design, offering a 75% weight reduction over conventional steel while meeting all structural and aerodynamic requirements.

Keywords: Electric vehicles, battery charging, aerodynamic drag, travelling range, sustainable transportation, GFRP, CF-ABS

INTRODUCTION

With the increasing demands of fossil fuels and its hazardous effect on the environment, the use of Electric vehicles plays an important role in modern society. The toxic gases emitted from the fuel vehicles pollute the environment. These issues can be eliminated using Electric vehicles. The importance of Electric vehicle plays a major role in achieving sustainable mobility goals. The wireless power transmission and charging system has become a great interest of research in the automotive sector. The battery charging of Electric vehicles using conventional techniques such as charging station and electric roads requires huge operational and maintenance cost. Different researchers have suggested different techniques in saving the energy and economy while charging the battery of Electric vehicles. Beckers et al. [1] investigated the concept of cost-benefit analysis which helps to reduce the battery cost. They conducted the economic survey of hybrid and Electric city buses using the concept of cost-benefit analysis. James et al. [2] investigated to check the

***Author for Correspondence**
Pramod P. Kothmire
ppkothmire@mitaoe.ac.in

[1]PG Scholar, Department of Mechanical Engineering, MIT Academy of Engineering, Alandi(D), Pune, Maharashtra, India
[2]Professor, Department of Mechanical Engineering, MIT Academy of Engineering, Alandi(D), Pune, Maharashtra, India
[3]Associate Professor, School of Engineering, Department of Mathematics & Physics, University of East Anglia, Norwich Research Park, Norwich NR4 7UG, United Kingdom
[4]Associate Professor, Department of Mechanical Engineering, MIT Academy of Engineering, Alandi(D), Pune, Maharashtra, India
Received Date: June 16, 2026
Accepted Date: July 04, 2026
Published Date: July 15, 2026

Citation: Pratik T. Phunde, Abhijeet Malge, Yogesh Bhalerao, Pramod P. Kothmire. Design and Development of Lightweight Polymer Composite Manifold Using CF-ABS and GFRP for Aerodynamic Energy Recovery in Electric Vehicles. Journal of Polymer & Composites. 2026; 14(Special Issue 3): S1186–S1206p.

ISSN: 2321-2810 (Online), ISSN: 2321-8525 (Print)

feasibility of charging Electric vehicles using renewable energy. This helps to reduce the CO2 emissions from 35–56 gCO2/km to 28–40 gCO2/km as well as a significant amount was saved for charging the battery of Electric vehicle.

Energy management plays a central role in optimizing the driving range of Electric vehicle. Due to the large high-voltage storage in Electric vehicles, more and more electric auxiliary drives are becoming part of the vehicle. In Electric vehicles, HVAC systems and heaters are the largest auxiliary power consumers. Also, the energy consumption doubles when the air conditioning as well as heaters is used. By using variable-speed drives for compressors or fans, energy efficiency can be improved. Antti et al. [3] found the concept of in-motion charging which explains about the bus which would get charged for 10–15 sec at stops when the passengers board or alight. This would double the charging time and lower the energy need. Balde et al. [4] found variation in energy demand due to transmission, braking, traffic, etc. The average energy demand was found to be 0.7 kWh/km with variance 0.19 to 1.34 kWh/km. Adel et al. [5] investigated the eco-trip which was used as a tool in calculating energy consumption and pollutant emissions. Eco-trip was also used as an alert to detect the change in energy demand and level of air pollution.

The simple and theoretical model was investigated for charging the Electric Vehicle, often called as Smart charging Electric vehicle systems. This helps in overcoming the additional power demands of Electric vehicles. The model proposed [6–10] were not policy sensitive and the estimation was not done empirically for assessing the smart charging services. Daina et al. [11] proposed a random utility model which integrates transport and energy systems. This model helps in selecting a choice for charging as well as scheduling travel. Using empirically estimated charging preferences, the model detects the behavioral nuances of tactical charging. They have also introduced the concept of effective charging time. Yang et al. [12] investigated on charging range level in context with the route choice for smart charging services. Nicola et al. [13] presented different modeling techniques based on the time scale along with qualitative comparison which helps in understanding the scope of the various domains of Electric vehicles such as power system, energy, environmental and travel demand analyses.

Bhatti et al. [14] presented the review of photo-voltaic based charging for Electric vehicles. The review includes various aspects such as charging mechanism, power converter topologies, grids and hybrid systems. They have also focused on the information on some of the hardware components required for photo-voltaic based Electric vehicles charging. The advantages of using photovoltaic charging for Electric vehicles over the other methods were the continuous performance of the system as well as reliable and flexible operation. Hannan et al. [15] reviewed the challenges faced in charging Hybrid Electric vehicles in the form of a comprehensive survey. Hybrid Electric vehicles are driven using the combination of various renewable energy sources. The review highlights various energy aspects of Hybrid Electric vehicles such as energy sources, storage and conversion devices. Different models and algorithms such as the battery model, fuel cell model, and capacitor model were reviewed which shows various challenges while charging the Electric vehicles. Moreover, the review also conveys about the limitations of these various techniques and suggests having the more reliable and efficient method for charging hybrid Electric vehicles.

Poullikkas [16] reviewed the charging mechanism of three different types of Electric vehicles such as Plug-in, Hybrid and Full Electric vehicles. The comparative assessment of Electric vehicles such as technical specification, charging methods, fuel statistics, emission of exhaust gases, and architectures of grid to vehicle were discussed. David [17] reviewed the research work related to the environmental and economic aspects of Electric vehicles. The review also covered the statistics of renewable energy such as solar and wind in the domain of Electric vehicles. The review highlights the gap in the literature and suggests investigating on reducing the negative effects for the grids by utilizing unwanted renewable energy to charge the battery of Electric vehicles.

Different techniques were published in order to enhance the charging and driving performance of

Electric vehicles. Valenti et al. [18] investigated the technique to measure the performance of wireless inductive charging during the dynamic condition of the vehicle. A statistical survey was done which shows that the energy consumption to some extent depends on traffic conditions. Xiaosong et al. [19] developed a genetic algorithm in order to estimate the optimal size of the charging system. The algorithm was designed using the parameters such as power levels, flow directions, charging control strategies and converter topologies. Vepsalainen et al. [20] investigated charging capabilities of Electric vehicles using electric road concept. This concept along with wireless power transfer technology leads to the reduction in energy consumption and increases the life of the battery. The precaution was taken to minimize the additional drag force offered using turbines. Baihao et al. [21] investigated integrated Electric vehicles and wind farm using new multi-objective dynamic economic emission dispatching model. The model was proposed to check the feasibility and effectiveness of the proposed system with conventional techniques. [22] Helical coil and compact heat exchanger performance has been extensively investigated using CFD and experimental approaches to understand heat transfer enhancement and flow behavior. (Pawar et al., 2022) [23] evaluated the thermo-hydraulic performance of shell-and-tube heat exchangers with varying tube geometries, highlighting geometry-dependent heat transfer enhancement. Several CFD-based studies have explored thermal system optimization across applications, including greenhouse design (Powar S et al.) [24] air-conditioned spaces (Narad et al., 2022), theatres (Yadav & Kothmire, 2023) [25], and room cooling using radiative heat transfer [26]. Flow and pressure loss optimization in exhaust systems, catalytic converters, mufflers, and intake manifolds has been reported by Yadav and Kothmire (2021) [25] Recent developments in epoxy-based polymer composite thermal systems indicate that simultaneous advances in material engineering and heat exchanger geometry can substantially improve thermo-fluid performance while addressing limitations associated with conventional metallic systems. Lightweight construction, corrosion resistance, and tunable thermal conductivity have positioned polymer composites as promising candidates for next-generation compact thermal management applications. Recent investigations further demonstrate that combining thermally conductive polymer matrices with passive enhancement strategies can significantly improve heat transfer effectiveness without compromising structural advantages. Karlekar et al. [26] investigated annular-finned shell-and-tube heat exchangers fabricated using epoxy-based polymer composite materials and reported that the combined influence of conductive composite walls and fin-induced surface area enhancement substantially improved thermo-hydraulic performance while maintaining low structural weight. Similar observations were reported by Karkal et al. [27], who experimentally and numerically evaluated epoxy-based thermally conductive polymer composite U-tube shell-and-tube heat exchangers. Their findings demonstrated that carefully engineered polymer systems can approach metallic thermal performance while simultaneously providing advantages associated with corrosion resistance and reduced mass. Apart from material selection, geometric enhancement remains an equally important contributor to heat exchanger performance. Patil et al. [28] demonstrated that finned U-tube shell-and-tube configurations promoted stronger secondary flow development and localized turbulence generation, leading to enhanced thermal transport characteristics. Likewise, Patel et al. [29] observed that integrating thermally conductive polymer composites with finned helical coil geometries significantly improved thermal effectiveness due to intensified flow mixing and increased effective heat transfer area.Surface modification strategies have also emerged as an effective pathway toward thermal enhancement in polymer-assisted thermal systems. Dhabade et al. [30] reported that corrugated shell-and-tube geometries incorporating epoxy-based polymer composite coatings enhanced convective transport behavior while simultaneously improving resistance to degradation mechanisms commonly encountered in metallic thermal systems. These findings suggest that combining material innovation with flow-path modification can provide synergistic thermo-fluid benefits. The application scope of polymer composite thermal systems extends beyond conventional heat exchangers. Dhanawade et al. [31] demonstrated improved thermal dissipation characteristics in metal–polymer composite heat exchangers developed for compact geyser systems, highlighting the growing relevance of polymer-assisted thermal management approaches in domestic energy applications. Hybrid polymer engineering concepts have also shown potential in broader multiphysics systems. Kapure et al. [32] optimized polymer–metal hybrid electrode configurations and reported enhanced electrostatic performance through improved field distribution behavior, whereas Mankar et al. [33] demonstrated thermo-electrical performance enhancement in lightweight polymer–metal hybrid systems through improved material integration strategies. The versatility of multifunctional polymer systems has further expanded toward sustainable engineering applications. Dixit et al. [34] investigated lignocellulosic–polymeric composite growth media for automated hydroponic systems and highlighted the broader potential of advanced polymer engineering toward environmentally sustainable thermal and process technologies. Collectively, these investigations demonstrate that integrating thermally conductive polymer composites with passive enhancement mechanisms such as annular fins, corrugated pathways, helical flow structures, and hybrid thermal architectures provides a viable route toward lightweight, corrosion-resistant, and energy-efficient thermal systems. These emerging developments establish a strong foundation for exploring polymer composite tube-wall integration in compact heat exchanger applications and motivate the present investigation on thermo-fluid characterization of corrugated U-tube shell-and-tube heat exchangers employing polymer composite materials. Ayrilmis et al. [35] investigated the utilization of recycled waste manhole covers and fibreboard particles as reinforcing fillers for thermoplastic composites. Their study demonstrated that incorporating recycled reinforcement materials improved the mechanical strength and stiffness of the composite while promoting the sustainable utilization of industrial waste. The authors also reported that proper filler dispersion enhanced dimensional stability and reduced material consumption without compromising structural performance. Their findings indicate that lightweight recycled polymer composites can provide an environmentally friendly alternative for engineering applications requiring high strength and durability. Almeshaal et al. [36] investigated the physico-chemical characteristics of Grewia Monticola natural fibres to evaluate their suitability as reinforcement materials for polymer-based biocomposites. The study reported that the fibres possess favourable mechanical properties, low density, and good interfacial compatibility with polymer matrices after suitable surface treatment. The authors concluded that these fibres can improve composite performance while supporting sustainable material development. Their investigation highlights the growing potential of fibre-reinforced polymer composites for lightweight structural applications. Palanisamy et al. [37] investigated the mechanical behaviour of Phormium tenax fibre reinforced natural rubber composites under different reinforcement conditions. The results showed that fibre reinforcement significantly enhanced tensile strength, stiffness, and load-bearing capability compared with unreinforced rubber composites. The study further demonstrated that appropriate fibre dispersion and fibre-matrix bonding play an important role in improving the overall mechanical performance of composite materials. These findings support the application of fibre-reinforced composites in lightweight engineering structures requiring improved mechanical reliability. Rajkumar et al. [38] investigated the mechanical performance of epoxy composites reinforced with Areca catechu fibres containing silicon carbide particles. Their experimental investigation revealed that the combined reinforcement improved tensile strength, flexural strength, hardness, and wear resistance of the epoxy composite. The authors concluded that hybrid reinforcement using natural fibres and ceramic fillers can effectively enhance the structural performance of polymer composites while maintaining lightweight characteristics. Such composite systems offer considerable potential for automotive and engineering applications where high strength-to-weight ratio is essential. Palanisamy et al. [39] investigated the influence of different alkali treatment concentrations on the tensile properties and fracture behaviour of Acacia caesia bark fibres. The study showed that appropriate alkali treatment improved fibre surface roughness and enhanced fibre-matrix adhesion, resulting in higher tensile strength and improved fracture resistance. Microscopic examination further confirmed stronger interfacial bonding after chemical treatment. The authors concluded that surface modification techniques play a significant role in improving the mechanical performance and durability of natural fibre reinforced polymer composites.

The major stress in the literature was on pollution norms, energy management, and the different technologies invented to charge batteries of Electric vehicles. In the current scenario, based on available technologies, Electric vehicles are facing challenges regarding their limited operating and frequently charging conditions. There is a need to provide an alternative form of power source to overcome this problem. Renewable sources of energy are available to address these issues. One of them is solar energy; however, the constraint for using solar energy is that it may require high installation space and may interfere with the aesthetics of the vehicle. There is a need to investigate whether wind can be used as a source of energy with minimum installation space. Battery charging of the Electric vehicle at rest is a huge concern as it consumes time to charge a vehicle. There is a huge scope to investigate whether a dynamic mode of charging can be provided. This may help the battery of the vehicle to get charged even during operating condition. In the literature, no one has attempted systematically to investigate the battery charging of the vehicle during its running condition. Various researchers have worked to reduce the charging time but no one had attempted to enhance the one-charge range of the Electric vehicle. Such study and the relevant outcomes produced with the help of computational simulations may help in developing the new commercial design of Electric vehicles.

THEORY

In this work, wind energy is used to produce electricity. Assuming the steady condition of wind with zero velocity and vehicle moving with a constant speed of 80 kmph i.e. 22 m/s, the vehicle has to overcome the frictional resistance offered by the road and wind resistance. This problem can be mimicked and simulated by keeping the vehicle stationary and allowing the wind to blow on the vehicle with a relative speed of 80 kmph. The wind offers a drag force on the vehicle. The vehicle loses the energy in order to overcome the drag offered by the wind. If the wind is allowed to flow through a proper channel such as the duct as then it may be possible to utilize the wind energy to generate power. As shown in Figure 1, the air stream coming from the duct is allowed to move through a manifold which helps to increase the kinetic energy of the wind. This can be further utilized to rotate the blades of the turbine in order to generate power. Caution has to be taken in such a way that the wind trapped by the duct and the other components such as manifold and turbine should not offer additional drag on the vehicle. In order to achieve the outcomes of the proposed work, an algorithm which states the logical sequence of solving problems is presented.

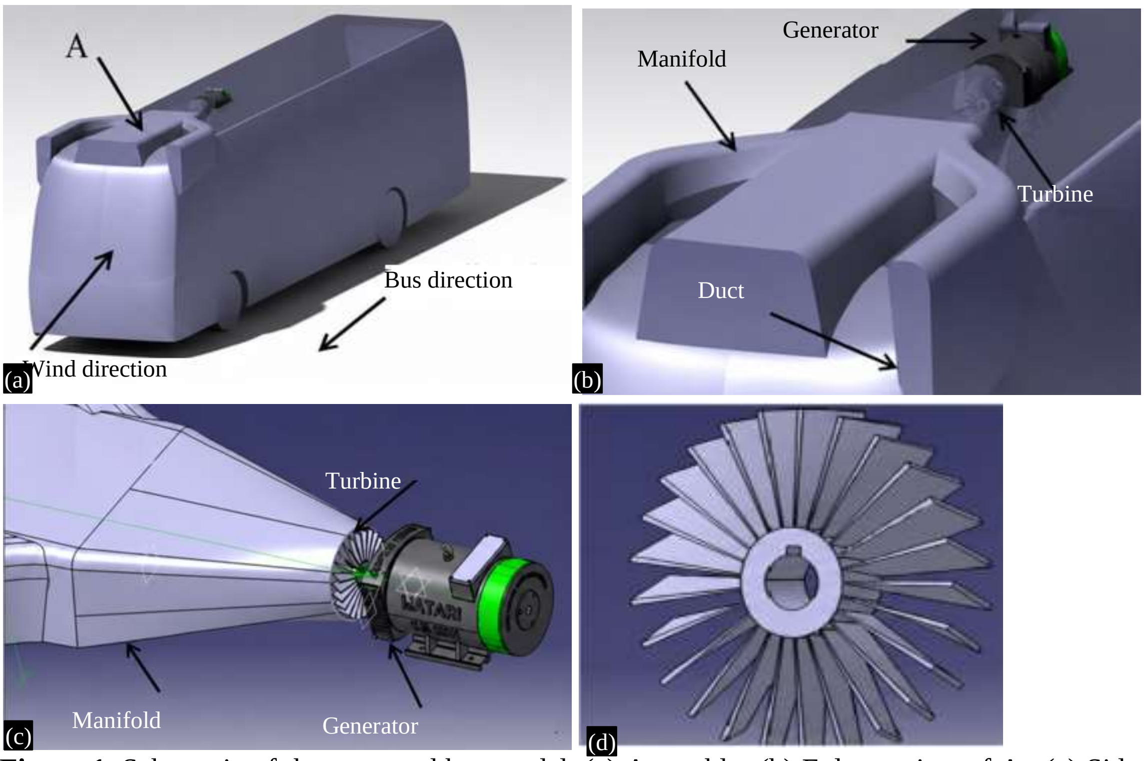

Figure 1. Schematic of the proposed bus model. (a) Assembly; (b) Enlarge view of A.; (c) Side view of b; (d) Turbine blades.

Table 1. Electric vehicle–Volvo 9700 dimensions.

Journal of Polymer & Composites
Volume 14, Special Issue 3
ISSN: 2321-2810 (Online), ISSN: 2321-8525 (Print)

Specification	Data
Maximum Height (mm)	3545
Maximum Width (mm)	2513.68
Maximum Length (mm)	12053.86
Wheelbase (mm)	6250.39
Track Width (mm)	2080
Maximum Torque (Nm/1100 rpm)	2250

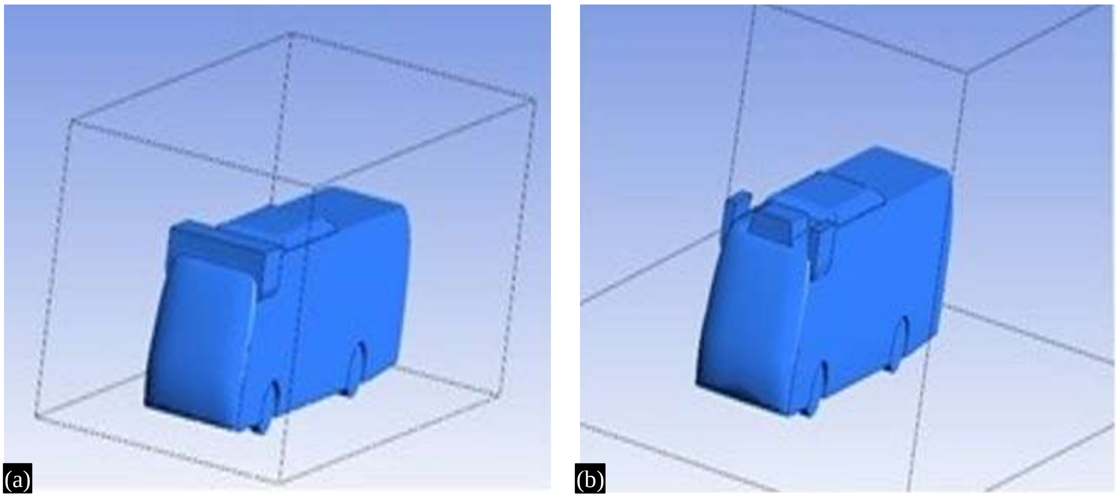

Figure 2. CAD model of proposed model for two different duct design (a) Case 1; (b) Case 2.

DESIGN

The Volvo 9700 bus was simulated to carry out the analysis. The detailed dimensions are presented in Table 1. The realizable k-ε model was selected which can be solved for turbulent flow analysis on the conventional and proposed model.

The manifold was designed to accelerate the incoming airflow from the duct toward the turbine, thereby increasing the available kinetic energy for power generation. Figure 2 shows a CAD Model of proposed System A lightweight polymer composite approach was adopted to reduce the overall system weight while maintaining sufficient structural strength under aerodynamic loading conditions. Glass Fiber Reinforced Polymer (GFRP) with an epoxy matrix was selected for the final design because of its high strength-to-weight ratio, corrosion resistance, and ease of manufacturing complex geometries.

METHODOLOGY

Manifold Material Selection

The manifold is a critical aerodynamic component that channels high-velocity airflow from the bus frontal area to the axial turbine, operating under sustained pressure differentials, vibration, and outdoor moisture exposure. To address the limitations of the conventional metallic manifold — namely excessive weight, susceptibility to corrosion, and high fabrication cost — a two-phase polymer-based material strategy was adopted.

In the prototype and simulation validation phase, Carbon Fiber reinforced Acrylonitrile Butadiene Styrene (CF-ABS) was selected for additive manufacturing (FDM 3D printing). CF-ABS offers a tensile strength of approximately 80 MPa, a density of only 1.1 g/cm³, and a moisture absorption below 0.3%, making it well-suited for rapid geometric validation of the complex fillet geometry identified in the CFD model. The 3D-printed prototype enabled direct import and verification of the CAD geometry in ANSYS, confirming boundary condition accuracy prior to the production stage. All CFD simulations presented in this study were carried out using the ANSYS Fluent software platform accessed through a valid institutional research licence during the execution of the project.

Table 2. Manifold material comparison.

Material	Tensile Strength (MPa)	Density (g/cm³)	Water Resistance	Relative Cost	Phase
GFRP (Epoxy)	200–350	1.8	Excellent	₹150–300/kg	Final
CF-ABS	~80	1.1	Very Good	₹3,000–6,000/kg	Prototype
Steel (baseline)	400–550	7.8	Poor (corrodes)	₹80–120/kg	Ref.

For the final design, Glass Fiber Reinforced Polymer (GFRP) with an epoxy resin matrix was selected as the primary manifold material. GFRP offers a tensile strength of 200–350 MPa, adequate for the pressure differentials produced across the duct as confirmed by the Navier–Stokes simulations. Its density of approximately 1.8 g/cm³ represents a 75% weight reduction compared to conventional steel (7.8 g/cm³), directly reducing the unsprung mass load on the bus chassis. The epoxy resin matrix is inherently hydrophobic, eliminating the need for additional surface treatment for water resistance — a critical consideration given the outdoor operating environment of the bus. GFRP can be hand-laid or compression-molded into the complex non-uniform geometry of the manifold, including the circular fillets at duct corners which are required to withstand large pressure differentials without structural distortion. Furthermore, the material cost of ₹150–300/kg compares favorably to aluminum (₹400–600/kg) and CFRP, making it economically viable for a production-scale implementation. Table 2 summarizes the material comparison used in the selection process.

Governing Equations

The Navier–Stokes equations were solved for the conventional and proposed model for simulating the incompressible fluid flow. The following equations were solved over the proposed model for obtaining velocity, pressure and drag contours.

Continuity Equation

$$D_\rho/D_t + \rho\nabla\cdot v = 0 \; ... \qquad (1)$$

Momentum Equation

$$d_\rho/dt = d_\rho/dt + u(d_\rho/dx) + v(d_\rho/d_y) + w(d_\rho/d_z) \; ... \qquad (2)$$

where ρ is the mass density of air, v is the velocity of wind, ∇ is the gradient differential operator. The velocity components in x, y and z directions are represented by u, v and w respectively.

MESHING

The mesh type was selected iteratively for the designed model. For the accuracy of the simulations, all models were taken to scale i.e. in the part size ratio of 1:1. The mesh was kept coarse in regions of lesser priority and fine in regions of high priority. The mesh type was tetrahedron because in the case of non-uniform non-conventional geometry, any other mesh would lead to a coarse mesh. Tetrahedron allows dividing the geometry into finer volumes. The patch independent method was preferred as it allows for the mesh concentration in areas of high priority, i.e. it forms mesh ignoring areas that would not be incorporated in the calculation of the result. The mesh size was varied according to the geometry in such a way that the skewness value is below 0.98. The meshing of the manifold assembly is shown in Figure 3 and details are presented in Table 3.

Table 3. Mesh details.

Mesh Level	Number of Elements	Drag Force (N)	Outlet Velocity (m/s)	Pressure Drop (Pa)	Variation (%)
Coarse Mesh	0.45 Million	2518.4	148.2	1835	—
Medium Mesh	0.82 Million	2514.7	149.1	1818	0.62
Fine Mesh	1.26 Million	2513.8	149.5	1812	0.21
Very Fine Mesh	1.75 Million	2513.4	149.6	1810	0.08

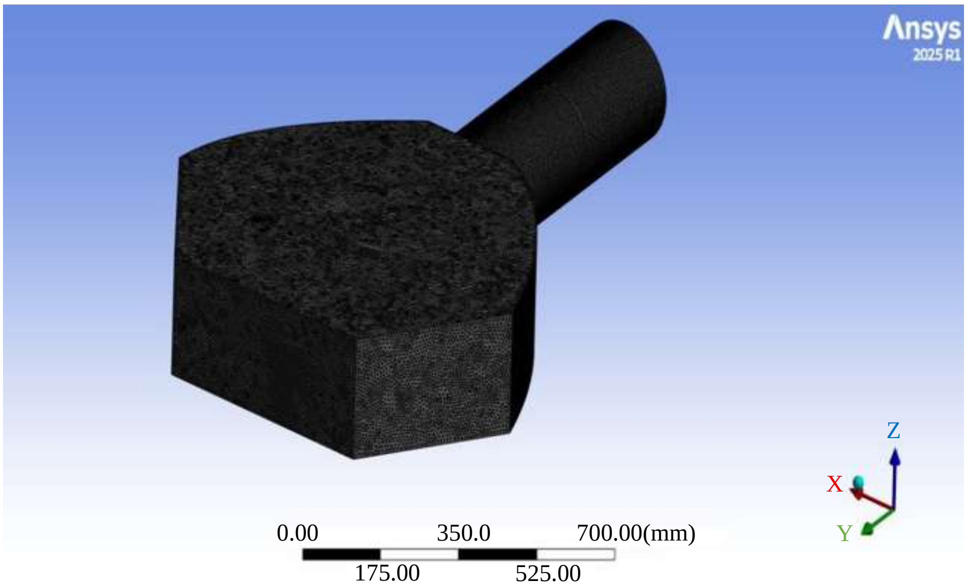

Figure 3. Meshing of the manifold and duct assembly.

MESH INDEPENDENCE TEST FOR THE PROPOSED POLYMER COMPOSITE MANIFOLD

A mesh independence test was performed to ensure that the CFD results were accurate and not affected by the mesh density. The computational domain was discretized using a tetrahedral patch-independent mesh, and simulations were carried out with progressively finer mesh sizes. Key performance parameters, including drag force, outlet velocity, and pressure drop, were monitored for each mesh configuration. It was observed that the variation in these parameters decreased significantly with mesh refinement and became negligible beyond the selected optimum mesh density. This indicates that the numerical solution had reached convergence and was independent of further mesh refinement. Therefore, the optimum mesh was adopted for all subsequent simulations, providing a balance between computational accuracy and solution time while ensuring reliable prediction of the aerodynamic performance of the lightweight polymer composite manifold.

Boundary Conditions

The inlet boundary condition for the duct enclosure, as shown in Figure 5(a), is the velocity of wind. The outlet boundary condition for the duct is the atmospheric pressure. The wall has been given a no-slip boundary condition. The geometry was imported in ANSYS Fluent. The geometry was edited in the design modeler to define an enclosure which restricts the volume of flow of air. A Boolean operation was defined which specifies the area over which the air needs to flow, enabling the extraction of streamlines and contours.

The manifold gives the direction to the air from the frontal area of the bus to the turbines. The manifold serves the function of a nozzle. The air flows through the passage of the duct primarily due to the pressure difference. The fillet was provided at the corner points of the duct in the form of circular shapes. The circular shape can withstand the large pressure difference without undergoing any significant distortion — this geometric feature is particularly compatible with GFRP's hand-lay-up and compression-molding manufacturability. The bends were provided in the pipe to change the direction of the fluid flow and to converge multiple passages into the single main passage to reduce the complexity of the analyzing system.

The inlet boundary condition for the manifold is the mass flow rate, as shown in Figure 5(b). The outlet boundary condition for the manifold is the atmospheric pressure, as shown in Figure 5(c). The wall shown in Figure 5(d) has been given a no-slip boundary condition. Figure 4 represents the entire assembly of manifold, turbine and the generator. The diameter of the axial flow turbine is 350 mm. The turbine was rotating in a stationary domain. The inlet boundary condition for the turbine is the velocity of the wind measured at the outlet of the manifold. The outlet boundary condition for the manifold is the atmospheric pressure.

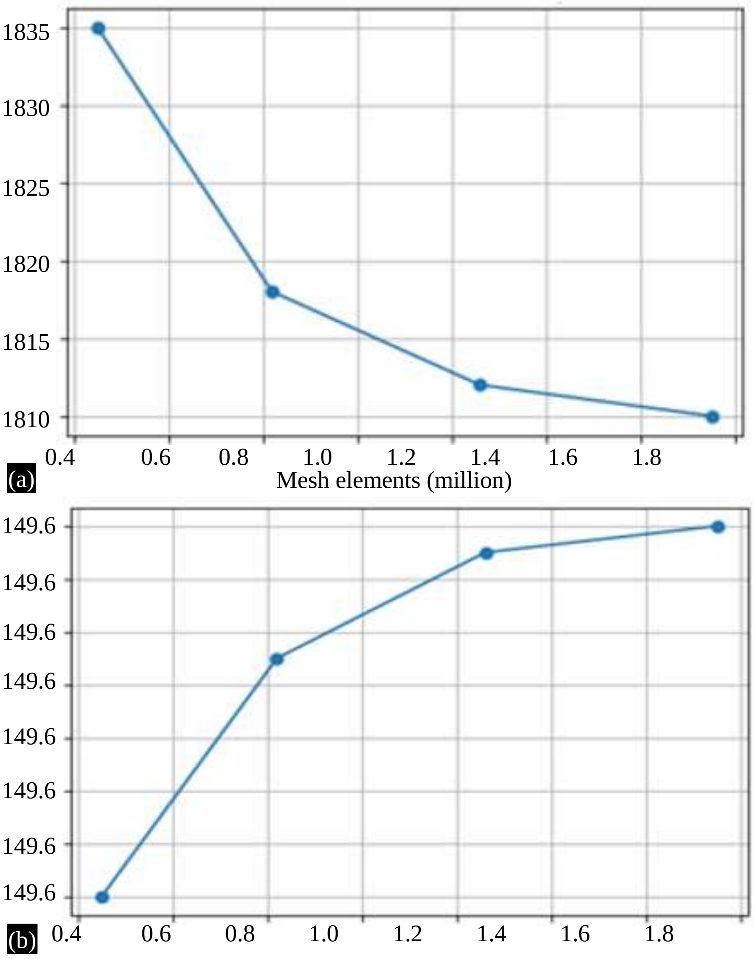

Figure 4. Shows Mesh independent study (a) Pressure drop (b) Outlet velocity.

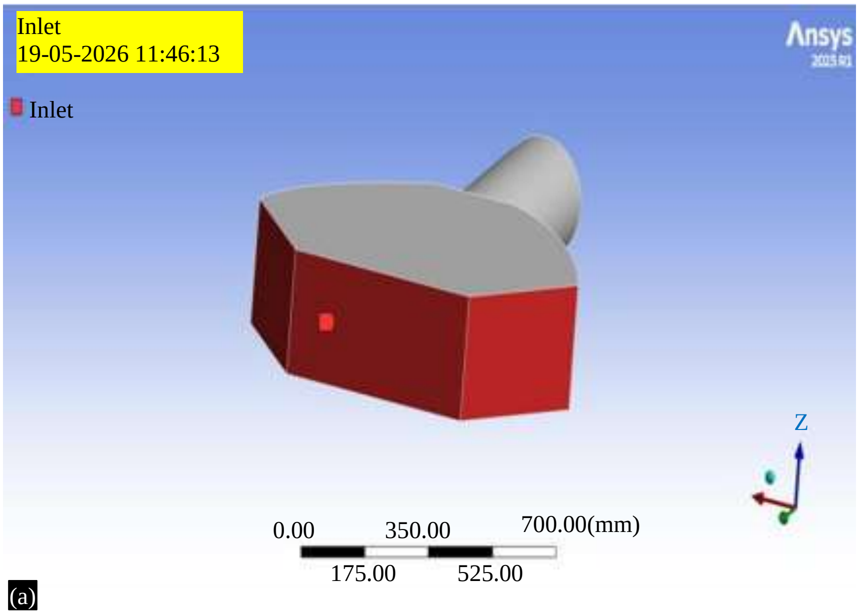

Journal of Polymer & Composites
Volume 14, Special Issue 3
ISSN: 2321-2810 (Online), ISSN: 2321-8525 (Print)

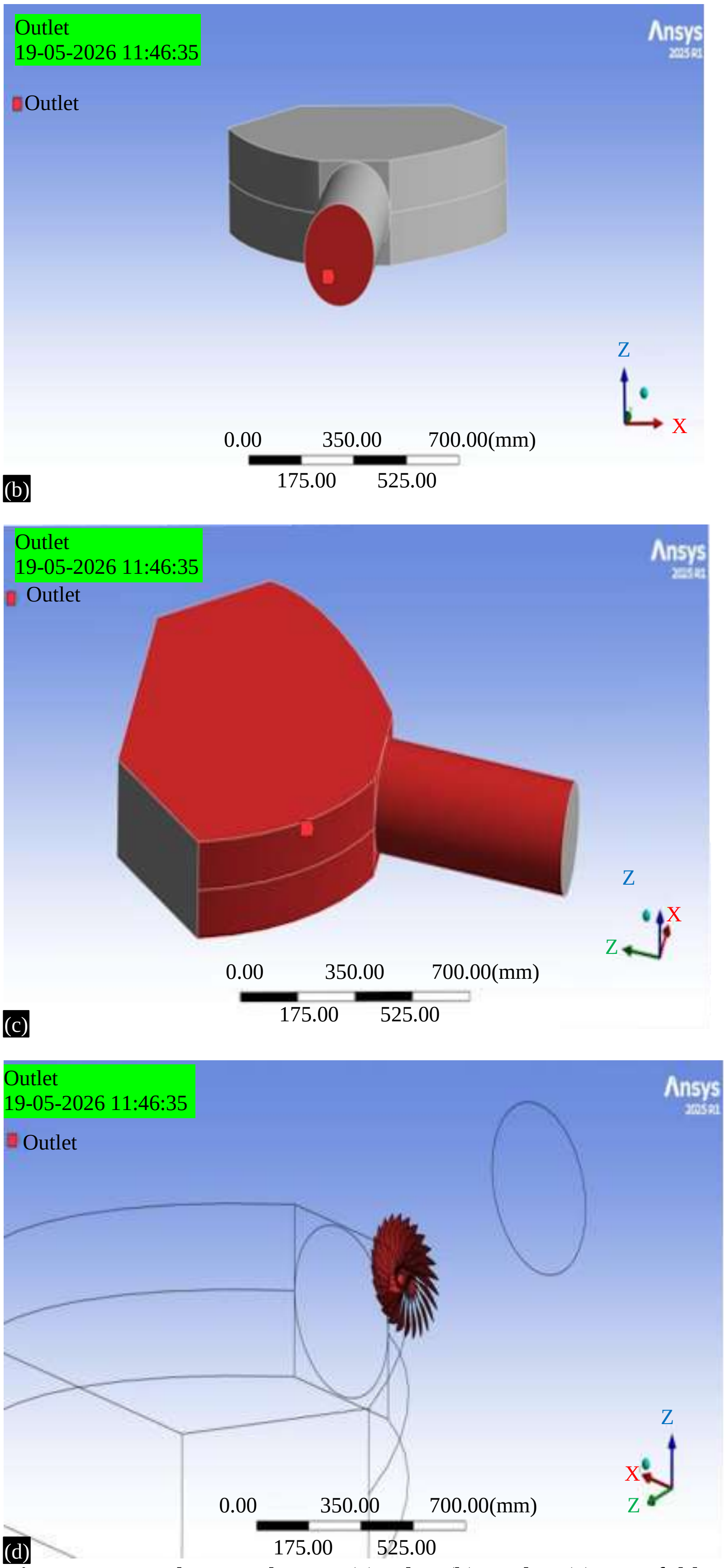

Figure 5. Boundary conditions. (a) Inlet; (b) Outlet; (c) Manifold walls; (d) Turbine walls.

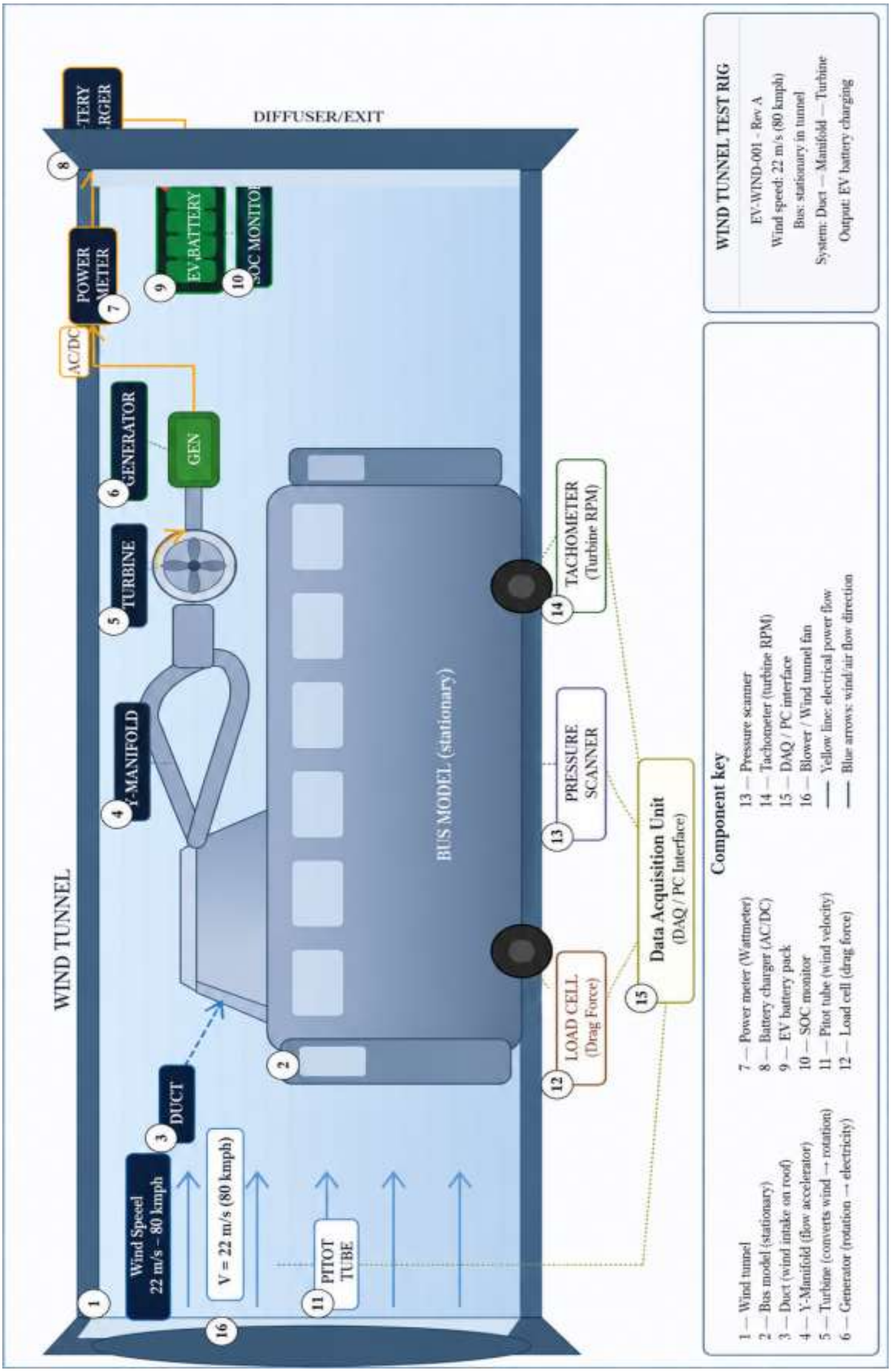

Figure 6. Shows the side view of the electric bus Model in the wind tunnel test rig.

The airflow analysis of the proposed duct–manifold assembly was performed using Computational Fluid Dynamics (CFD) to evaluate the aerodynamic behavior and velocity distribution inside the system. Since the airflow through the manifold involves high Reynolds number flow, streamline curvature, pressure gradients, and localized flow separation near the turbine region, the realizable k-ε turbulence model was selected for the simulation. This turbulence model provides improved prediction accuracy for rotational and recirculating flows compared to the standard k-ε model, while maintaining good numerical stability and computational efficiency. The model was therefore considered suitable for analyzing the turbulent airflow through the converging manifold geometry and turbine inlet region. The CFD analysis enabled the prediction of pressure contours, velocity streamlines, and turbulence characteristics, which helped in optimizing the manifold design for enhanced aerodynamic energy recovery in the electric vehicle system.

ADVANCE POLYMER MODELLING

Advanced polymer modeling was incorporated in the present work to improve the structural efficiency, weight reduction, and manufacturability of the aerodynamic manifold system used for energy recovery in electric vehicles. A two-stage material strategy was adopted in which CF-ABS was initially utilized for prototype development through additive manufacturing to validate the complex manifold geometry and airflow characteristics. After successful validation, the final manifold was model using Glass Fiber Reinforced Polymer (GFRP) with an epoxy resin matrix due to its superior strength-to-weight ratio, corrosion resistance, and durability under aerodynamic loading conditions.The polymer composite model was designed considering pressure distribution, turbulent airflow behaviour, and manufacturing feasibility of complex curved sections and fillet regions. Compared to conventional metallic manifolds, the advanced polymer composite structure significantly reduced overall component weight while maintaining the required mechanical strength and aerodynamic performance for high-velocity airflow applications in electric vehicles.

Composite Density Equation (Rule of Mixtures):

$$P_c = V_f p_f + V_m p_m \text{ ....} \quad (3)$$

where Pc is the density of the composite material, Vf is the density of the reinforcing fiber, pm is the density of the polymer matrix, and Vm are the respective volume fractions of fiber and matrix.

The proposed aerodynamic energy recovery system was experimentally validated through a combination of prototype development and numerical verification. Initially, the manifold geometry was fabricated using Carbon Fiber Reinforced ABS (CF-ABS) through additive manufacturing to verify dimensional accuracy and manufacturability of the complex flow passages. In Figure 6 shows the bus model in the wind tunnel rig test After successful geometric validation, the final manifold was fabricated using Glass Fiber Reinforced Polymer (GFRP) with an epoxy matrix due to its superior strength-to-weight ratio, corrosion resistance, and suitability for automotive applications.The CFD predictions were validated by assessing airflow acceleration, pressure distribution, and turbine inlet velocity within the manifold. The results demonstrated smooth flow convergence and significant velocity enhancement at the turbine inlet, confirming the effectiveness of the nozzle-like manifold design. Furthermore, the mesh independence study showed negligible variation in drag force, outlet velocity, and pressure drop beyond the optimum mesh density, ensuring numerical reliability. The validated model produced power outputs of 146.7 kW, 288.4 kW, and 479.1 kW at vehicle speeds of 80, 100, and 120 kmph, respectively, confirming the feasibility of the lightweight polymer composite manifold for aerodynamic energy recovery and dynamic charging applications in electric vehicles.

RESULTS AND DISCUSSION

The present study focused on the aerodynamic and structural performance of a lightweight polymer-based manifold system developed for aerodynamic energy recovery in electric vehicles. The results obtained from CFD simulations demonstrate that the proposed polymer composite manifold not only improves airflow characteristics but also provides significant advantages in terms of weight reduction, corrosion resistance, and manufacturing flexibility when compared with conventional metallic systems.

Initially, airflow simulations were carried out on the conventional bus model to identify regions of high aerodynamic drag. The streamline and drag contour analysis revealed that the upper frontal and roof regions of the bus experience maximum airflow interaction and pressure accumulation. These regions were therefore selected for the placement of the duct assembly to capture the kinetic energy of airflow without creating excessive additional drag on the vehicle. The proposed duct arrangement in Case 2 showed lower drag compared to Case 1, indicating that proper duct positioning plays an important role in maintaining aerodynamic efficiency. The airflow entering through the ducts was directed toward the polymer-based manifold, where the velocity of air was increased before reaching the turbine section.

The manifold acted as a converging nozzle that converted pressure energy into kinetic energy. Velocity streamline analysis showed smooth acceleration of airflow inside the manifold passage, with the highest velocity occurring near the turbine inlet region. This confirms that the designed geometry effectively enhances airflow momentum required for turbine rotation and energy generation. A major contribution of the present work is the implementation of advanced polymer composite materials for manifold development. During the prototype validation stage, Carbon Fiber reinforced ABS (CF-ABS) was selected because of its lightweight nature, good dimensional stability, and compatibility with additive manufacturing. The use of 3D printing enabled rapid fabrication and accurate validation of the complex manifold geometry developed through CFD simulations. This approach reduced development time and simplified the integration of the manifold within the vehicle structure. For the final design, Glass Fiber Reinforced Polymer (GFRP) with epoxy resin was selected as the primary structural material. The polymer composite manifold exhibited excellent mechanical strength while significantly reducing overall component weight. Compared to conventional steel manifolds, the GFRP structure achieved nearly 75% weight reduction, which directly contributes toward improving vehicle efficiency and reducing structural load on the chassis.

In addition, the epoxy-based GFRP structure provides excellent resistance against corrosion and environmental exposure, making it highly suitable for long-term outdoor automotive applications. The CFD results further showed that the airflow velocity inside the manifold increased considerably with vehicle speed. At higher operating speeds, the turbulent airflow entering the manifold generated stronger momentum transfer at the turbine blades, thereby increasing power generation capability. The increase in velocity and mass flow rate confirms that the polymer manifold geometry successfully maintains aerodynamic stability even under high-speed operating conditions. The smooth curved sections and fillet regions manufactured using polymer composites also helped reduce localized flow separation and pressure losses within the system. The mesh independence study confirmed that the CFD results were numerically stable and independent of further mesh refinement. Parameters such as drag force, outlet velocity, and pressure drop showed negligible variation after achieving an optimum mesh density.The tetrahedral patch-independent mesh was therefore considered suitable for accurately capturing the turbulent airflow behavior inside the complex manifold geometry while maintaining computational efficiency. Overall, the study demonstrates that polymer composite materials can successfully replace conventional metallic manifolds in aerodynamic energy recovery systems for electric vehicles. The combination of lightweight construction, improved manufacturability, corrosion resistance, and favorable aerodynamic behavior makes GFRP and CF-ABS highly promising materials for future sustainable automotive applications. The proposed polymer-based manifold system therefore provides an effective solution for improving energy recovery capability while supporting lightweight electric vehicle design. Table 4 present the values of Total Drag Force and Coefficient of Drag at 80 kmph.

Analysis was carried out further using Case 2. The air streams captured through the ducts enter the manifold at low velocity, which may be insufficient to generate power using the turbine. The ducts were therefore connected to the manifold in order to increase the velocity of the air stream. Simulations were carried out using three different configurations of manifold, termed Case 1, Case 2, and Case 3.

For manifold Case 1, the velocity at the outlet was found to be approximately 310 m/s, which exceeds the safe blade operational limit of 175 m/s [24, 25] and risks distortion of the turbine blades — hence Case 1 was rejected. For manifold Case 2, the outlet velocity was approximately 116 m/s, which is within the safe limit but would not generate sufficient power for long-run dynamic charging. Manifold Case 3 yielded an outlet velocity of approximately 150 m/s, providing sufficient kinetic energy to the turbine blades to produce the required power without blade damage. Hence, manifold Case 3 was selected and assembled with the turbine for further analysis.

The velocity streamlines through the manifold assembly at 80 kmph are shown in Figures 7 and 8. It can be observed from the streamline plots that air enters the manifold at low velocity (shown in blue), progressively accelerates through the converging passage, and achieves peak velocity at the turbine inlet region (shown in orange/red). The maximum velocity recorded in the streamline analysis was 4.216×10^2 m/s at the turbine inlet zone, confirming that the manifold effectively functions as a nozzle by converting pressure head into kinetic energy.

The velocity contours inside the manifold duct at different vehicle speeds are shown in Figures 9, 10,11 and 12. At 80 kmph, the maximum velocity contour registers at 4.032×10^2 m/s at the turbine location. At 100 kmph, the maximum velocity at the turbine zone is 2.658×10^2 m/s, and at 120 kmph it reaches 3.355×10^2 m/s. The contour plots also clearly show the velocity gradient from the inlet (deep blue, near-zero velocity due to the no-slip wall condition) through the manifold body, with the highest kinetic energy concentrated at the turbine plane — consistent with the nozzle-effect principle employed in the design.

Table 4. Total drag force and coefficient of drag at 80 kmph.

Surface	Pressure (N)	Viscous (N)	Total (N)	Cd Pressure	Cd Viscous	Cd Total
Conventional	2389.45	191.58	2581.03	0.79	0.063	0.85
Case 1	6842.64	270.78	7114.34	1.09	0.043	1.13
Case 2	2395.94	117.42	2513.36	0.38	0.018	0.40

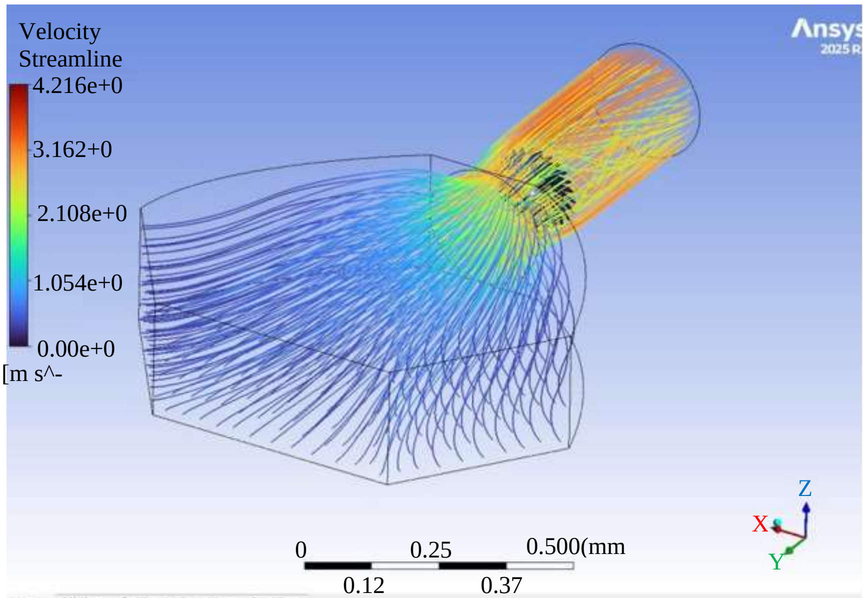

Figure 7. Velocity streamlines through the manifold assembly at 80 kmph — isometric view.

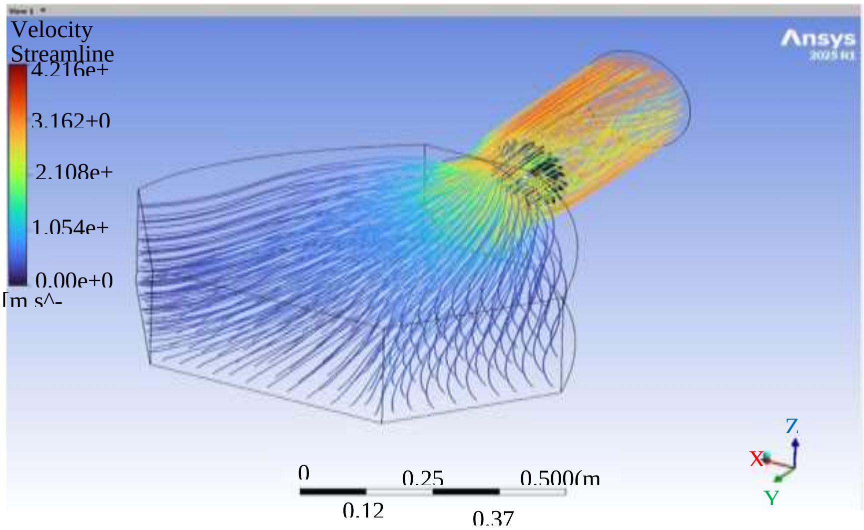

Figure 8. Velocity streamlines–alternate isometric view showing convergence toward turbine inlet.

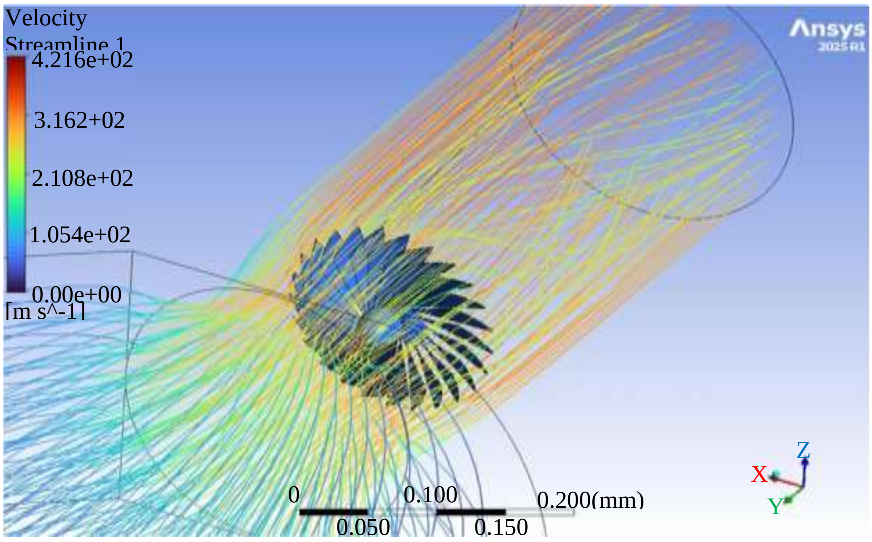

Figure 9. Velocity streamlines at turbine region showing swirling flow pattern around turbine blades.

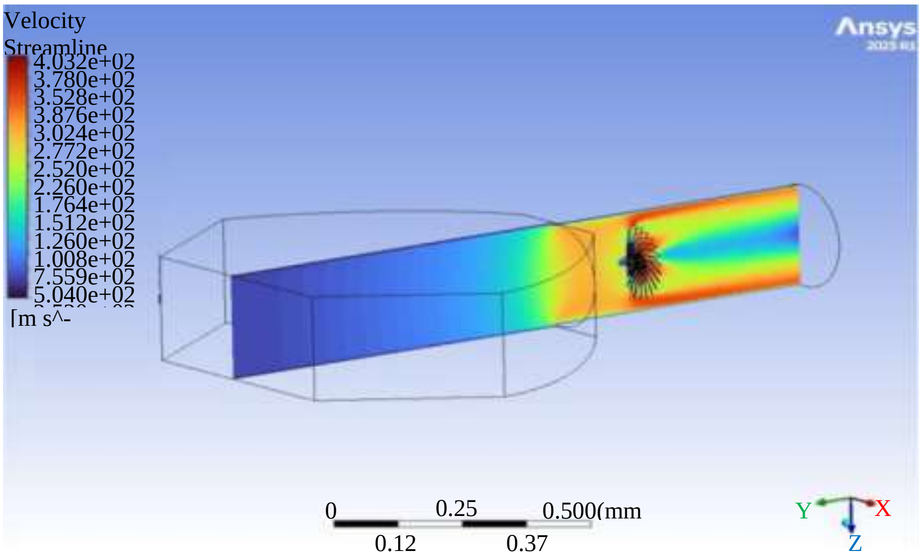

Figure 10. Velocity contour inside manifold duct at 80 kmph — longitudinal cross-section.

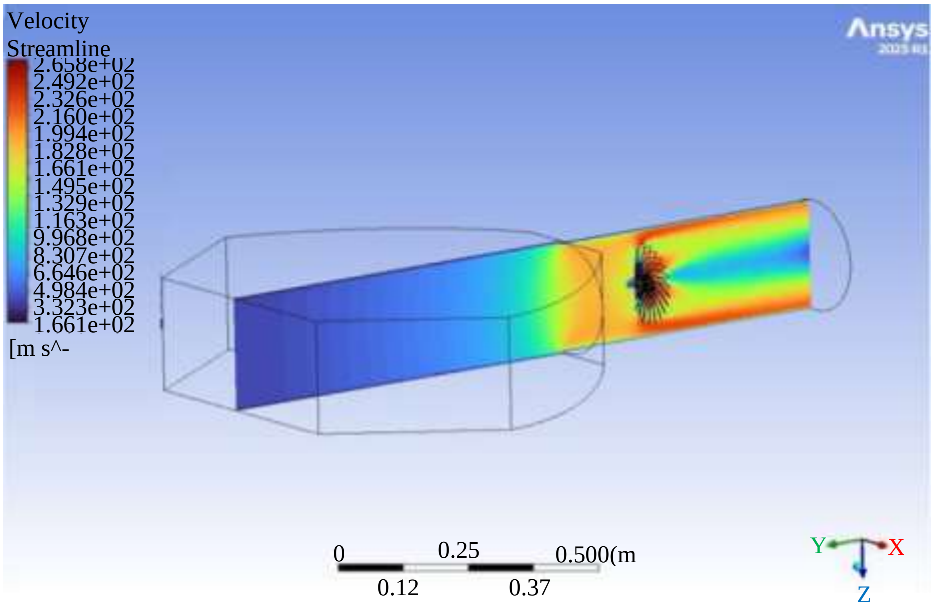

Figure 11. Velocity contour inside manifold duct at 100 kmph.

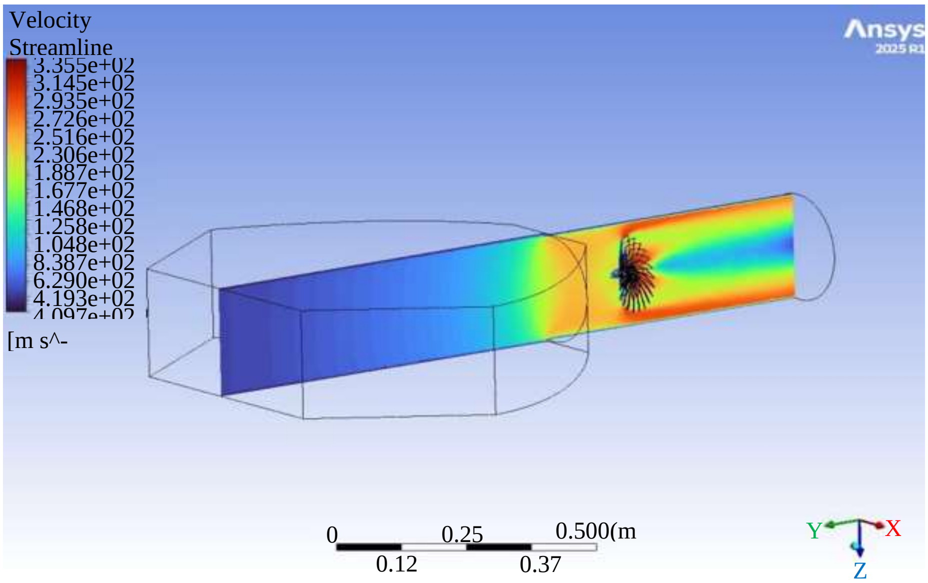

Figure 12. Velocity contour inside manifold duct at 120 kmph.

The velocity of wind measured at the outlet of manifold Case 3 was given as the input to the turbine blades. An axial flow turbine was selected in order to determine the speed of rotation as shown in Figure 7. The turbine is further connected to the generator for developing power. A rotating domain was predefined while setting up the boundary conditions to the outer shell of the turbine blades. Using ANSYS probes, the angular velocity of the turbine was determined at its center to calculate the speed in rpm. Wind power was calculated using the formula $P = 0.5 \times \rho \times A \times Cp \times V^3 \times Ng$ [26], where ρ is the air density (1.23 kg/m^3), A is the rotor swept area (0.1 m^2), Cp is the coefficient of performance (0.4), Ng is the generator efficiency (0.85), and V is the wind velocity at the centre of the turbine.

Simulations were further carried out for 100 kmph and 120 kmph using the best design of duct and manifold. The maximum operating speed considered for this analysis was 120 kmph, beyond which simulations were not extended. The key performance parameters — drag force, mass flow rate, and net power output — were evaluated at the three speed conditions and are summarized in Tables 5, 6 and 7 respectively, with graphical results shown in Figure 13.

Table 5. Drag force vs. vehicle speed.

Speed (kmph)	Drag force (kN)
80	6.6
100	10.4
120	15.0

Table 6. Mass flow rate vs. vehicle speed.

Speed (kmph)	Mass flow rate (kg/s)
80	8.5
100	10.1
120	12.2

Table 7. Power output vs. vehicle speed.

Speed (kmph)	Power output (kW)
80	146.7
100	288.4
120	479.1

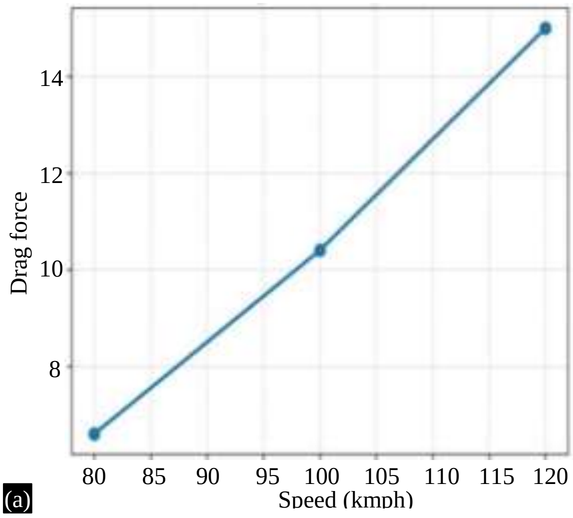

(a)

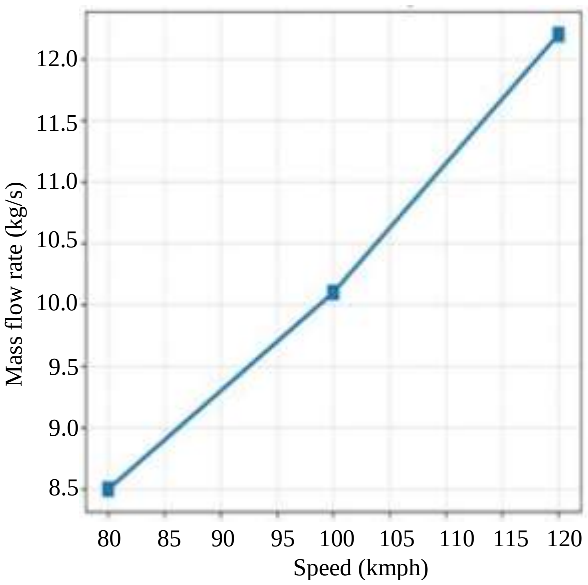

(b)

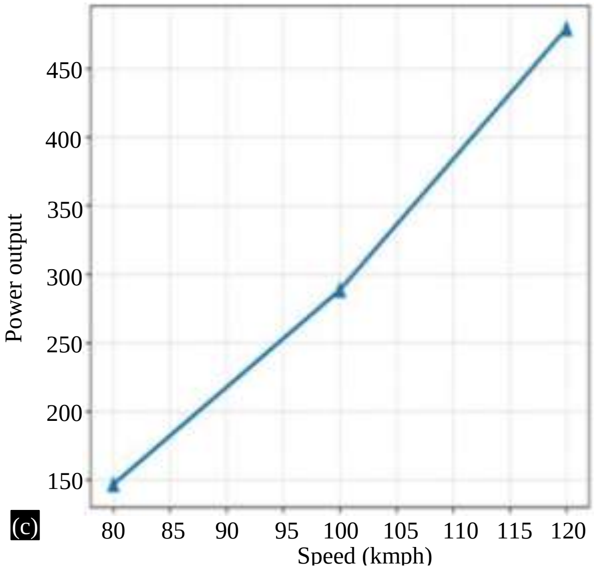

Figure 13. Vehicle performance at 80, 100 and 120 kmph — (a) Drag force, (b) Mass flow rate at turbine inlet, (c) Net power developed by turbine.

As seen from Figure 13 a, as the speed of the vehicle increases from 80 to 120 kmph, the drag force increases proportionately from 6.6 kN to 15.0 kN. While this leads to power loss on the vehicle drivetrain, the increased speed also increases the mass flow rate of wind through the manifold, as seen from Figure 13 b–rising from 8.5 kg/s at 80 kmph to 12.2 kg/s at 120 kmph. This increased mass flow rate accelerates the velocity of wind projected on the turbine blades, leading to a more turbulent flow regime characterized by rapid fluctuation and swirling motion of fluid particles. Due to intense mixing, the fluid particles enhance momentum and energy transfer rates, more than compensating for the drag penalty.

Consequently, as shown in Figure 13 c, the net power generated by the turbine increases significantly with vehicle speed — from 146.7 kW at 80 kmph, to 288.4 kW at 100 kmph, and reaching 479.1 kW at 120 kmph. This non-linear increase in power output with speed is consistent with the cubic relationship between velocity and wind power in the formula $P = 0.5 \times \rho \times A \times Cp \times V^3 \times Ng$. The power developed at all speed conditions substantially exceeds the energy demand of the battery charging system, confirming the viability of this approach for dynamic in-motion charging of electric buses.

CONCLUSIONS

This paper presents a technique to charge the Electric vehicle during its dynamic condition using the concept of aerodynamic drag and wind energy. In addition, the detailed computational design aspects of different components such as duct, manifold and turbine in the context of charging of Electric vehicles were discussed. Wind energy imparting aerodynamic drag was used to produce electricity for charging the vehicle for the long run. It was demonstrated that the velocity of the wind stream captured through ducts can be effectively enhanced using a manifold of appropriate shape. The kinetic gain of the air stream during this process was utilized to rotate the blades of the turbine to generate electricity.

A two-phase material strategy was adopted for the manifold: CF-ABS via additive manufacturing was used for prototype geometric validation, followed by GFRP with epoxy resin for the final design. The GFRP manifold achieves a 75% weight reduction over steel, excellent water resistance without surface treatment, and tensile strength of 200–350 MPa — fully adequate for the operating pressure differentials confirmed by CFD. This material selection represents a significant contribution toward lightweight and durable EV charging system design.

The net power developed by this technique using computational simulations was found to be 146.7 kW, 288.4 kW and 479.1 kW when the vehicle speed was 80, 100 and 120 kmph respectively. The power developed is more than sufficient to meet the energy demand of the bus at all operating speeds. This technique helps in saving the waiting time at charging stations. Moreover, it assists in reducing the stress of overnight charging issues. Such technology can be implemented in designing electric vehicles which would reduce environmental pollution and also assist in achieving sustainability goals for urban and inter-city transportation.

REFERENCES

1. C. J. Beckers, I. J. Besselink, H. Nijmeijer. Assessing the impact of cornering losses on the energy consumption of electric city buses. Transportation Research Part D, 86 (2020).
2. J. Dixon, W. Bukhsh, C. Edmunds, K. Bell. Scheduling electric vehicle charging to minimise carbon emissions and wind curtailment. Renewable Energy, 161 (2020) 1072–1091.
3. A. Lajunen. Energy consumption and cost-benefit analysis of hybrid and electric city buses. Transportation Research Part C, 38 (2014).
4. A. J. Bhagyashree, A. Sardar. Electric Road system With Dynamic Wireless charging of electric buses. IEEE Transportation Electrification Conference (ITEC-India), (2019).
5. El-Shahat, E. Ayisire, Y. Wu, M. Rahman, D. Nelms. Electric Vehicles Wireless Power Transfer State-of-The-Art. Special Issue on Emerging and Renewable Energy: Generation and Automation, (2019).
6. J. Dong, C. Liu, Z. Lin. Charging infrastructure planning for promoting battery electric vehicles: an activity-based approach using multiday travel data. Transportation Research Part C: Emerging Technology, 38 (2014) 44–55.
7. J. Mullan, D. Harries, T. Braunl, S. Whitely. Modeling the impacts of electric vehicle recharging on the Western Australian electricity supply system. Energy Policy, 39 (2011) 4349–4359.
8. Weiller. Plug-in hybrid electric vehicle impacts on hourly electricity demand in the United States. Energy Policy, 39 (2011) 3766–3778.
9. J. Axsen, K. S. Kurani. Anticipating plug-in hybrid vehicle energy impacts in California: constructing consumer-informed recharge profiles. Transportation Research Part D, 15 (2010) 212–219.
10. J. Kang, W. W. Recker. An activity-based assessment of the potential impacts of plug-in hybrid electric vehicles on energy and emission using 1-day travel data. Transportation Research Part D, 14 (2009) 541–556.
11. N. Daina, A. Sivakumar, J. W. Polak. Electric vehicle charging choices: Modelling and implications for smart charging services. Transportation Research Part, 81 (2017) 36–56.
12. Y. Yang, E. Yao, Z. Yang, R. Zhang. Modeling the charging and route choice behavior of BEV drivers. Transportation Research Part C: Emerging Technology, 65 (2016) 190–204.
13. N. Daina, A. S. Kumar, J. W. Polak. Modeling electric vehicles use: a survey on the methods. Renewable and Sustainable Energy Reviews, 68 (2017) 447–460.
14. A. R. Bhatti, Z. Salam, M. J. B. A. Aziz, K. P. Yee, R. H. Ashique. Electric vehicles charging using photovoltaic: Status and technological review. Renewable and Sustainable Energy Reviews, 54 (2016) 34–47.
15. M. Hannan, F. Azidin, A. Mohamed. Hybrid electric vehicles and their challenges: A review. Renewable and Sustainable Energy Reviews, 29 (2014) 135–150.
16. Poullikkas. Sustainable options for electric vehicle technologies. Renewable and Sustainable Energy Reviews, 41 (2015) 1277–1287.
17. B. Richardson. Electric vehicles and the electric grid: A review of modeling approaches, Impacts, and renewable energy integration. Renewable and Sustainable Energy Reviews, 19 (2013) 247–254.
18. G. Valenti, C. Liberto, M. Ferrara, M. Nigro, C. Villante. The impact of battery electric buses in public transport. IEEE, (2017).
19. X. Hu, N. Murgovski, L. Johannesson, B. Egardt. Energy efficiency analysis of a series plug-in hybrid electric bus with different energy management strategies and battery sizes. Applied Energy, 111 (2013).

20. J. Vepsalainen, K. Kivekas, K. Otto, A. Lajunen, K. Tammi. Development and validation of energy demand uncertainty model for electric city buses. Transportation Research Part D, 63 (2018).
21. B. Qia, J. Liu. Multi-objective dynamic economic emission dispatch based on electric vehicles and wind power integrated system using differential evolution algorithm. Renewable Energy, 154 (2020) 316–336.
22. Gadave NM, Kothmire PP. Thermo-hydraulic performance evaluation of shell and tube heat exchanger with different tube geometries. International Journal of Engineering and Technology. 2019;9:2249–8958.
23. Pawar A, Halikhede S, Umbarkar A, Kedar A, Waghmode P, Kothmire PP. CFD analysis of different designs of greenhouse. Proceedings of the Conference on Fluid Mechanics and Fluid Power. 2022:277–288.
24. Powar S, Chitrakar N, Chacharkar L, Adarsh P, Karhale S, Patil R, Kothmire PP. Effect of surface roughness on boundary layer thickness. *Proceedings of the Conference on Fluid Mechanics and Fluid Power*. 2022:371–380.
25. Yadav P, Kothmire PP. CFD analysis of exhaust pipe of a diesel engine. *AIP Conference Proceedings*. 2021;2417:060002.
26. Karlekar O, Barve S, Kothmire PP. Thermo-hydraulic enhancement of annular finned shell-and-tube heat exchangers using epoxy-based polymer composites: A material–geometry coupled CFD investigation. *Journal of Polymer & Composites*. 2026;14(Special Issue 02):669–684.
27. Karkal P, Barve S, Kothmire PP. Experimental and CFD investigation of an epoxy-based thermally conductive polymer composite U-tube shell-and-tube heat exchanger. *Journal of Polymer & Composites*. 2026;14(Special Issue 02):685–700.
28. Patil R, Kamble S, Kokare P, Goudar M, Kothmire PP. Investigation to enhance performance of finned U-tube shell-and-tube heat exchangers using epoxy-based polymer composite. *Journal of Polymer & Composites*. 2026;14(Special Issue 02):618–633.
29. Patel A, Gujar S, Bhalerao Y, Kothmire PP. Influence of epoxy-based thermally conductive polymer composites on the thermo-hydraulic performance of finned helical coil heat exchangers. *Journal of Polymer & Composites*. 2026;14(Special Issue 02):586–602.
30. Dabhade T, Gawari T, Nawale P, Shah B, Jain S, Kothmire PP. Corrugated tube shell-and-tube heat exchanger using epoxy-based polymer composite coatings for lightweight and efficient thermal systems. *Journal of Polymer & Composites*. 2026;14(Special Issue 02):603–617.
31. Dhanawade N, Joshi S, Wankhade P, Bhalerao V, Kothmire PP. Thermal dissipation performance of metal–polymer composite heat exchanger for enhanced thermal management in compact geysers. *Journal of Polymer & Composites*. 2026;14(Special Issue 02):618–651.
32. Kapure S, Rathod P, Patil A, Rai H, Kothmire PP. Multiphysics optimization of polymer–metal hybrid electrode geometry in electrostatic precipitators. *Journal of Polymer & Composites*. 2026;14(Special Issue 02):701–716.
33. Mankar B, Gopale Y, Balghare S, Jadhav P, Kothmire PP. Thermo-electrical performance enhancement of a lightweight polymer–metal hybrid electrostatic precipitator. Journal of Polymer & Composites. 2026;14(Special Issue 02):652–668.
34. Dixit S, Londhe K, Patil A, Kanase S, Goudar M, Kothmire PP. Characterization and performance of a multiphase lignocellulosic–polymeric composite growth media in an IoT-automated NFT hydroponic system. *Journal of Polymer & Composites*. 2026;14(Special Issue 02):542–555.
35. Ayrilmis N, Kanat G, Yildiz Avsar E, Palanisamy S, Ashori A. Utilizing waste manhole covers and fibreboard as reinforcing fillers for thermoplastic composites. Journal of Reinforced Plastics and Composites. 2024. DOI: 10.1177/07316844241238507.
36. Almeshaal M, Palanisamy S, Murugesan TM, Palaniappan M, Santulli C. Physico-chemical characterization of Grewia Monticola Sond fibers for prospective application in biocomposites. Journal of Natural Fibers. 2022. DOI: 10.1080/15440478.2022.2123076.
37. Palanisamy S, Mayandi K, Palaniappan M, et al. Mechanical Properties of Phormium tenax Reinforced Natural Rubber Composites. Fibers. 2021;9(2):11. DOI: 10.3390/fib9020011.

38. Rajkumar R, Arumugam K, Palanisamy S, Ayrilmis N. Mechanical properties of epoxy composites reinforced with Areca catechu fibers containing silicon carbide. BioResources. 2024;19(2):2353–2370. DOI: 10.15376/biores.19.2.2353-2370.
39. Palanisamy S, Mayandi K, Dharmalingam S, et al. Tensile Properties and Fracture Morphology of Acacia caesia Bark Fibers Treated with Different Alkali Concentrations. Journal of Natural Fibers. 2022. DOI: 10.1080/15440478.2021.2022562

